

Enhanced photocatalytic activity of porous cerium titanate using PEG4000 in sol-gel route

LILI YANG, DA CHEN, JIAYING ZHANG, ZHAO LV, WENJIE ZHANG*

School of Environmental and Chemical Engineering, Shenyang Ligong University, Shenyang 110159, China

Polyethylene glycol was added in the sol-gel precursor to prepare porous cerium titanate. The cerium titanate samples are composed of brannerite structured CeTi_2O_6 of monoclinic system and a small proportion of cubic CeO_2 . FT-infrared and FT-Far infrared spectra demonstrate the surface adsorbed water molecules and metal-oxide bonds in the materials. The BET specific surface areas of the nonporous and porous cerium titanates are 1.7 and 16.2 m^2/g , and the pore volume of these two samples are 0.0036 and 0.0232 cm^3/g , respectively. The chemical shift of oxygen and titanium atoms in the porous cerium titanate is not found after using PEG4000. The first order reaction rate constant for photocatalytic degradation of ofloxacin on the nonporous sample is $1.340 \times 10^{-2} \text{ min}^{-1}$, while it is as high as $6.852 \times 10^{-2} \text{ min}^{-1}$ on the porous cerium titanate.

(Received April 21, 2018; accepted October 9, 2019)

Keywords: Cerium Titanate, Photocatalysis, PEG4000, Ofloxacin, Degradation

1. Introduction

Many kinds of hazardous organic pollutants in the environment can be decomposed via photocatalytic oxidation since photocatalyst can produce oxidative reagents upon light irradiation [1-3]. The main research focus in this field is the development of novel and active materials [4-6], including the most applied titania and other kinds of materials [7-9]. The properties of titanate are quite different since the cation can be alkaline earth metals, rare earth elements and even transition metals, and the prepared titanates may be in perovskite, ilmenite or other structures. R. Abe et al. prepared $\text{Y}_2\text{Ti}_2\text{O}_7$ and $\text{Gd}_2\text{Ti}_2\text{O}_7$ for hydrogen evolution from photocatalytic splitting of water [10]. H. Xue et al. proved methyl orange decomposition on pyrochloro-structured $\text{Gd}_2\text{Ti}_2\text{O}_7$, $\text{Nd}_2\text{Ti}_2\text{O}_7$ and $\text{Er}_2\text{Ti}_2\text{O}_7$ under illumination [11]. Verma et al. prepared microstructured CeTi_2O_6 thin films to examine the photocatalysis and electrochemical properties [12]. Otsuka-Yao-Matsuo et al. prepared CeTiO_4 and CeTi_2O_6 photocatalysts to degrade methylene blue in the aqueous solution [13].

Crystallization of lanthanide titanates usually occurs at high temperature and is necessary in solid state reaction, sol-gel route and hydrothermal method. The obtained materials are lack of porous structure due to particles aggregation and agglomeration during high temperature treatment. In order to introduce porous structure in the material, polyethylene glycol (PEG) was added in the precursor as template agent during sol-gel preparation of porous cerium titanate in this work. Since the use of template agent to synthesize porous lanthanide titanate is still a novel attempt, the obtained porous cerium titanate was compared with the nonporous cerium titanate to examine the differences in physicochemical properties, e.g. crystallization states, surface morphology, porous structure

and elemental environment.

Antibiotics in the wastewater of pharmaceutical plants are among the most concerned hazardous pollutants that have to be removed from the wastewater before discharging. These harmful substances can hardly be removed through the traditional bio-chemical technique. Deep oxidation methods such as photocatalysis are used to deal with most kinds of hazardous organic substances. Ofloxacin in the wastewater can also be degraded during photocatalytic oxidation process [14-16]. Photocatalytic degradation of ofloxacin under illumination in presence of the materials was examined to show the role of PEG4000 on enhancing the activity of the cerium titanate.

2. Experimental

2.1. Preparation of cerium titanate

The porous and nonporous cerium titanates were synthesized through a sol-gel route, in which two precursors were prepared before mixing them together. One precursor contained 0.85 mL tetrabutyl titanate and 8 mL ethanol, while the other precursor contained 8 mL deionized water, 8 mL acetic acid and 0.4652 g $\text{Ce}(\text{NO}_3)_3 \cdot 6\text{H}_2\text{O}$. 3.5 g PEG4000 was added in the second precursor to prepare the porous cerium titanate. The two precursors and 2 mL glycol were mixed to form the initial sol, and then the sol-gel transformation process was conducted in a 70 °C water bath. After dehydration of the gel at 110 °C, crystallization of the final product was performed at 800 °C for 3 h.

2.2. Characterization of the materials

X-ray powder diffraction patterns were taken on D8 X-ray diffractometer equipped with Cu $K\alpha$ radiation. Surface morphologies of the materials were measured by FEI Tecnai G2 20 transmittance electron microscope. Infrared and far infrared absorption spectra were determined by Frontier FT-IR/FIR spectrometer. Specific surface area and pore size distribution were examined on ASAP 2460 surface area and pore size analyzer [17]. Chemical environment of element was analyzed by ESCALAB 250Xi X-ray photoelectron spectroscopy with a monochromatic Al $K\alpha$ source.

2.3. Photocatalytic degradation

Photocatalytic degradation of ofloxacin on the porous and nonporous cerium titanates were examined in a lab-scale photocatalytic device that was made of a quartz reactor and a 20 W UV source. The illumination intensity at 253.7 nm on the surface of the reactor was 2300 $\mu\text{W}/\text{cm}^2$. The mixture of 20 mg CeTi_2O_6 and 50 mL 20 mg/L ofloxacin solution was irradiated for as long as 50 min to determine the degradation efficiency of ofloxacin. An Agilent 1260 HPLC was used to measure the concentration of the ofloxacin solution during photocatalytic degradation process. The chromatography column was ZorbaxEclipse XDB-C18 (150 \times 4.6 mm), and the mobile phase was the mixture of acetonitrile and 1% phosphoric acid aqueous solution.

3. Results and discussion

Fig. 1 shows XRD patterns of nonporous cerium titanate and porous cerium titanate. Both of the two cerium titanate samples are mainly composed of brannerite structured CeTi_2O_6 that belongs to monoclinic system [18]. The most preferred orientation is the (110) plane situating at the diffraction angle of $2\theta=26.1^\circ$. The crystallite size of the CeTi_2O_6 crystals on the preferred (110) plane is calculated through Scherrer equation, i.e. $\tau = K\lambda/(\beta \cdot \cos\theta)$, where τ is the mean size of the ordered (crystalline) domains, K is a dimensionless shape factor, λ is the X-ray wavelength, β is the line broadening at half the maximum intensity (FWHM), and θ is the Bragg angle. The crystallite sizes for the nonporous and porous cerium titanate samples are 31.9 and 38.0 nm, indicating the strengthened crystallization of brannerite CeTi_2O_6 crystals after adding PEG4000 template in the precursor.

As can be seen in the XRD pattern of the nonporous cerium titanate, there is a weak diffraction peak situating at $2\theta=56.3^\circ$, which can be attributed to cubic CeO_2 (JCPDS 43-1002). Weight percentage of CeO_2 in the materials was calculated using Relative Intensity Ratio. The nonporous sample contains 4.7% CeO_2 and 95.3% CeTi_2O_6 , and the porous sample contains 5.7% CeO_2 and 94.3% CeTi_2O_6 . The addition of PEG4000 in the precursor can affect the formation of both CeTi_2O_6 and CeO_2 . As a

result, crystal growth of both monoclinic CeTi_2O_6 and cubic CeO_2 are enhanced in the porous cerium titanate sample.

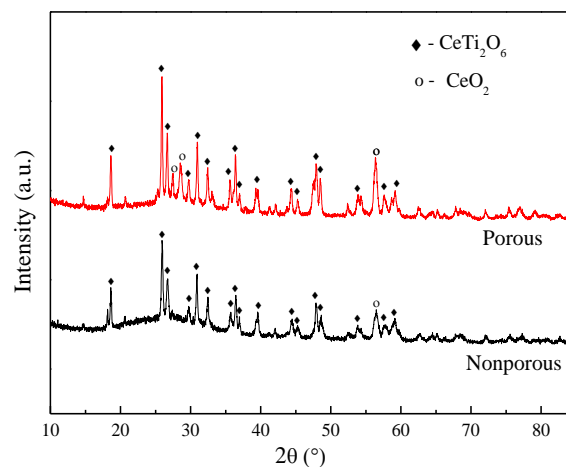


Fig. 1. XRD patterns of nonporous cerium titanate and porous cerium titanate

The transmittance electron microscope (TEM) surface morphologies of the nonporous cerium titanate and porous cerium titanate samples are presented in Fig. 2. Apparently, the nonporous sample is in the aggregated form of cerium titanate particles and there is hardly any porous structure in the large particle. On the contrary, the porous sample can be easily dispersed before TEM examination and there is no particles aggregation in the image. Interparticle holes can be clearly found in the image, since the removal of PEG4000 molecules during calcination may leave pores in the material. The existence of PEG4000 in the precursor and the gel successfully retards the aggregation of small cerium titanate particles into larger ones.

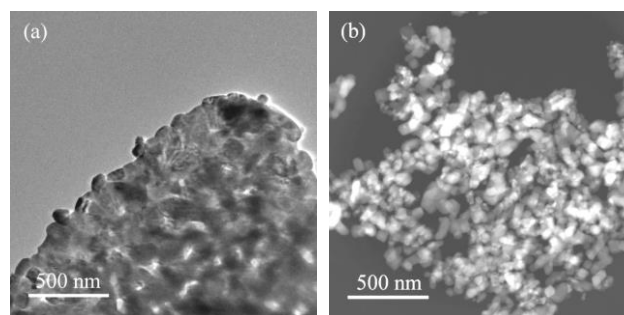


Fig. 2. TEM images of (a) nonporous cerium titanate and (b) porous cerium titanate

FT-infrared and FT-Far infrared spectra of nonporous cerium titanate and porous cerium titanate are illustrated in Fig. 3 to ascertain the chemical bondings in the materials. The absorption peaks at 3440 and 1631 cm^{-1} for stretching and bending vibrations of hydroxyl group indicate the surface adsorbed water molecules [19]. The absorption intensities of hydroxyl group on the porous sample are greater than the nonporous sample because more water

molecules can be adsorbed on the porous material. The bending vibration of Ti-O bond at 670 cm^{-1} and the stretching vibration of Ti-O-Ti bond at 514 cm^{-1} can be observed in the FT-IR spectra [12].

Meanwhile, more absorptions of metal-oxide bonds in the materials can be distinguished in the FT-Far IR spectra. The overlapping of different vibration absorption peaks of Ti-O and Ce-O bonds makes up the complex far infrared spectra of the cerium titanate samples, as shown in Fig. 3(b). The absorption peaks situating at 272 and 405 cm^{-1} are attributed to stretching and bending vibrations of Ce-O bond, while the absorptions around 361 and 235 cm^{-1} belong to stretching and bending vibrations of Ti-O bond [20]. These absorption intensities are strengthened after using PEG4000 in sol-gel preparation of the porous cerium titanate.

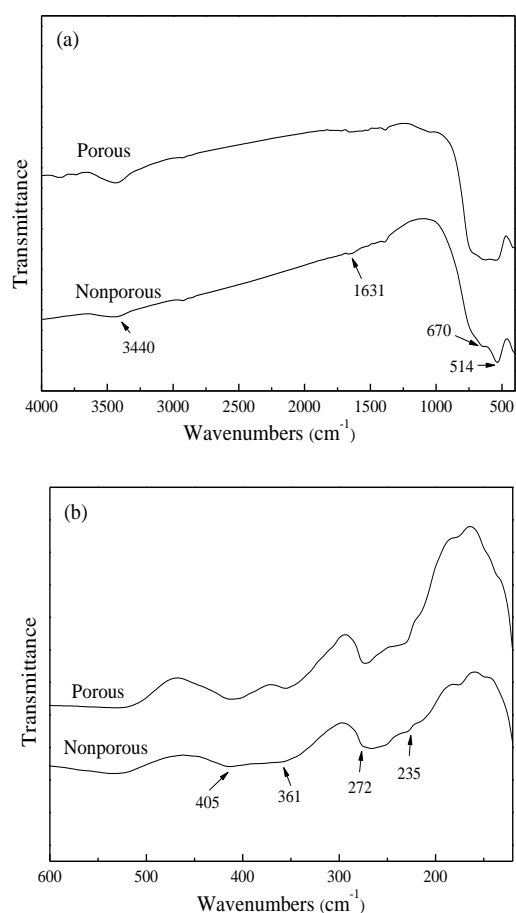


Fig. 3. FT-IR (a) and FT-Far IR (b) spectra of nonporous and porous cerium titanates

Fig. 4 illustrates N_2 adsorption-desorption isotherms and pore size distribution curves of nonporous and porous cerium titanates. As shown in Fig. 4(a), the total N_2 adsorption amount is apparently enhanced for the porous material. Both of the N_2 adsorption-desorption isotherms are regarded as IUPAC IV type, showing the mesoporous structure in the cerium titanate samples. The N_2 adsorption amount increases constantly with rising N_2 partial pressure in most of the pressure range, while there is a rapid

increase of the adsorbed N_2 amount when the relative pressure is higher than 0.95. The N_2 adsorption-desorption isotherms of the two samples contain a type H3 hysteric loop, which is related to wide pore size range in the samples. As can be seen from Fig. 4(b), pore size in the materials distributes from near-micropore to macropore.

BET specific surface area and total pore volume in the samples are calculated from Fig. 4. The BET specific surface areas of the nonporous and porous cerium titanate samples are 1.7 and $16.2\text{ m}^2/\text{g}$, and the pore volumes of these two samples are 0.0036 and $0.0232\text{ cm}^3/\text{g}$, respectively. As indicated by TEM images, the nonporous cerium titanate particles tend to aggregate into large particle without porous structure. The BET surface area and pore volume are quite small without using PEG4000 in the precursor. The addition of PEG4000 molecules in the precursor can obviously produce pores in the porous cerium titanate sample after calcination. The existence of PEG4000 not only enhances crystallization of brannerite CeTi_2O_6 crystals, but also retards the aggregation of small CeTi_2O_6 particles.

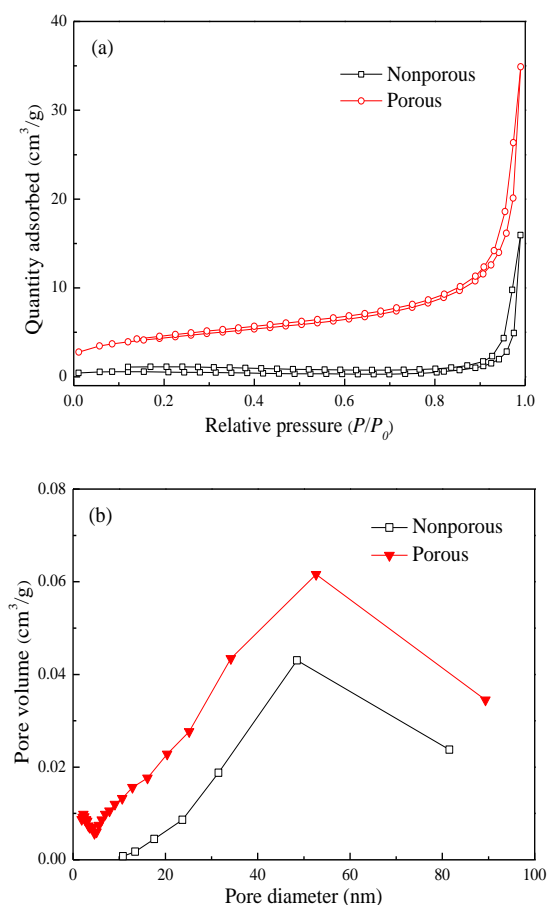


Fig. 4. (a) N_2 adsorption-desorption isotherms and (b) Pore size distribution curves of nonporous and porous cerium titanate samples

Fig. 5 presents XPS $\text{Ce}3d$, $\text{Ti}2p$ and $\text{O}1s$ spectra of the cerium titanate samples. Eight binding energy peaks can be distinguished in the $\text{Ce}3d$ spectra, in which peaks u and v correspond to $\text{Ce}3d_{5/2}$ and $\text{Ce}3d_{3/2}$ electron orbitals, and

the other peaks are the satellite peaks [21]. Alternatively, C. M. Teodorescu et al. reported the "shake-up" and "shake-down" satellites in $Ce3d$ XPS spectrum to identify different ionization states of cerium [22]. Quantitative analysis of the relative ratio of Ce^{3+} and Ce^{4+} in the materials can be obtained using the formula $Ce^{3+}(\%) = 100 \times (Sv + Su) / \sum(Sv + Su)$ [23]. The relative percentage of Ce^{3+} decreases from 19.4% in the nonporous cerium titanate to 16.5% in the porous cerium titanate sample. Cerium ions are mostly in the fourth oxidation state in the obtained cerium titanates, and this tendency is further strengthened after using PEG4000 in the precursor.

The three electrons binding energy peaks at 529.3, 529.8 and 530.9 eV are assigned to oxygen in cerium titanate lattice skeleton, oxygen molecule adsorbed on the surface of the sample, and oxygen in C-O bonds [24,25]. The $Ti2p_{1/2}$ and $Ti2p_{3/2}$ electrons have the binding energies at 463.9 and 458.2 eV in both of the two samples. Titanium is in the oxidation state of Ti^{4+} since the binding energy difference between $Ti2p_{1/2}$ and $Ti2p_{3/2}$ electrons is 5.7 eV [23]. The chemical shift of oxygen and titanium atoms in the porous cerium titanate is not found after using PEG4000.

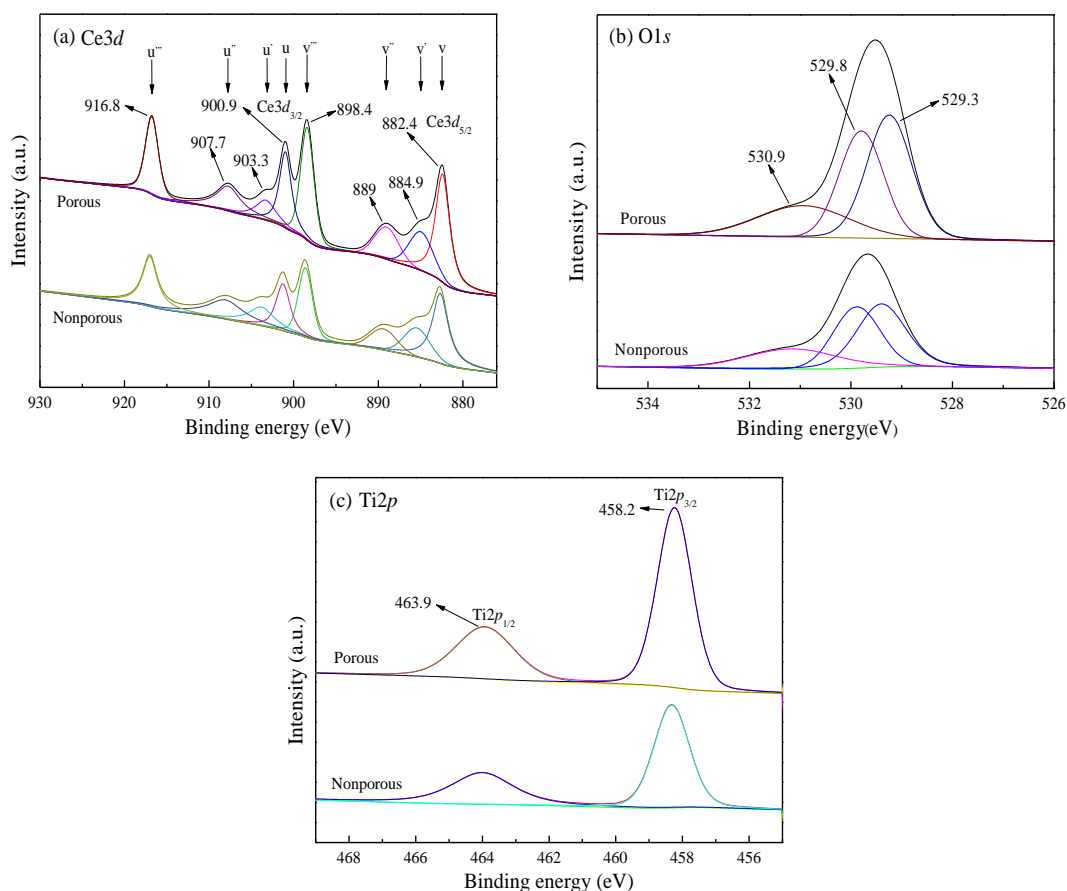


Fig. 5. XPS spectra of nonporous cerium titanate and porous cerium titanate

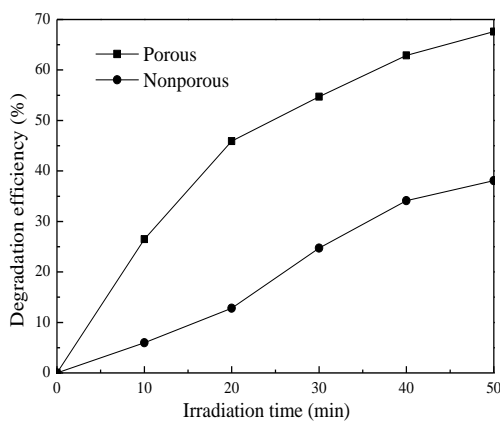


Fig. 6. Ofloxacin photocatalytic degradation with prolonged irradiation time on nonporous cerium titanate and porous cerium titanate samples

Ofloxacin can be adsorbed on the surface of the materials and the maximum removal efficiencies are 12.5% and 27.6% on the nonporous and porous samples, respectively. Meanwhile, photocatalytic degradation is the only pathway leading to decomposition of hazardous organic substance. Photocatalytic activity of the materials are compared after 50 min of irradiation and the results show that as much as 38.1% and 67.6% of the initial ofloxacin molecules can be degraded on the nonporous and porous cerium titanate samples. The first order reaction rate constant for photocatalytic degradation of ofloxacin on the nonporous sample is $1.340 \times 10^{-2} \text{ min}^{-1}$, while it is as high as $6.852 \times 10^{-2} \text{ min}^{-1}$ on the porous cerium titanate. The relative percentage of Ce^{3+} decreases from 19.4% in the nonporous cerium titanate to 16.5% in the porous cerium titanate sample. This small difference cannot be the major origin of the improved photocatalytic activity. The enhancement in photocatalytic activity can be mostly attributed to the enlarged surface area and pore volume in the porous cerium titanate sample. As stated before, the BET specific surface areas of the nonporous and porous cerium titanate samples are 1.7 and $16.2 \text{ m}^2/\text{g}$, and the pore volumes of these two samples are 0.0036 and $0.0232 \text{ cm}^3/\text{g}$, respectively.

4. Conclusions

The influences of PEG4000 on the properties of cerium titanate were investigated in this work. The addition of PEG4000 in the precursor can promote crystallite formation of both the majority CeTi_2O_6 and the minority CeO_2 . The use of PEG4000 successfully retards the aggregation of small cerium titanate particles into larger ones. The vibration absorptions of Ti-O and Ce-O bonds in the cerium titanate samples can be ascertained in the far infrared spectra. The addition of PEG4000 molecules in the precursor can obviously produce pores in the porous cerium titanate sample after calcination. Both of adsorption capacity and photocatalytic activity of cerium titanate are apparently enhanced in the porous material.

Acknowledgments

This work was supported by National Natural Science Foundation for Youths of China (No. 51504154), Research on Basic Science and Technology in Universities Supported by Education Department of Liaoning Province (No. LG201706), and Scientific Research Project of Education Department of Liaoning Province (No. LG201913).

References

- [1] M. R. Hoffmann, S. T. Martin, W. Choi, W. Bahnemann, *Chem. Rev.* **95**, 69 (1995).

- [2] A. Fujishima, T. N. Rao, D. A. Tryk, *J. Photochem. Photobio. C* **1**, 121 (2000).
- [3] W. J. Zhang, Y. J. Tao, C. G. Li, *Mater. Res. Bull.* **105**, 55 (2018).
- [4] D. Pang, L. Qiu, Y. Wang, R. Zhu, F. Ouyang, *J. Environ. Sci.* **33**, 169 (2015).
- [5] G. Plantard, T. Janin, V. Goetz, S. Brosillon, *Appl. Catal. B* **115–116**, 38 (2012).
- [6] W. J. Zhang, Y. X. Liu, C. G. Li, *J. Phys. Chem. Solids* **118**, 144 (2018).
- [7] W. J. Zhang, Z. Ma, L. Du, L. Yang, X. Chen, H. He, *J. Alloys Compds.* **695**, 3541 (2017).
- [8] F. Li, K. Yu, L. Lou, Z. Su, S. Liu, *Mater. Sci. Eng. B* **172**, 136 (2010).
- [9] J. Chen, S. Liu, L. Zhang, N. Chen, *Mater. Lett.* **150**, 44 (2015).
- [10] R. Abe, M. Higashi, K. Sayama, Y. Abe, H. Sugihara, *J. Phys. Chem. B* **110**, 2219 (2006).
- [11] H. Xue, Y. W. Zhang, J. Xu, X. P. Liu, Q. R. Qian, L. Xiao, Q. Chen, *Catal. Commun.* **51**, 72 (2014).
- [12] A. Verma, A. Goyal, R. K. Sharma, *Thin Solid Films* **516**, 4925 (2008).
- [13] S. Otsuka-Yao-Matsuo, T. Omata, M. Yoshimura, *J. Alloys Compds.* **376**, 262 (2004).
- [14] A. Kaur, G. Gupta, A. O. Ibhaddon, D. B. Salunke, A. S. K. Sinha, S. K. Kansal, *J. Environ. Chem. Eng.* **6**, 3621 (2018).
- [15] G. Gupta, A. Umar, A. Kaur, S. Sood, A. Dhir, S. K. Kansal, *Mater. Res. Bull.* **99**, 359 (2018).
- [16] W. J. Zhang, Y. J. Tao, C. G. Li, *J. Photochem. Photobio. A: Chem.* **364**, 787 (2018).
- [17] S. Brunauer, P. H. Emmett, E. Teller, *J. Am. Chem. Soc.* **60**, 309 (1938).
- [18] A. Verma, A. K. Srivastava, K. N. Sood, *Solid State Ionics* **178**, 1288 (2007).
- [19] W. J. Zhang, K. L. Wang, Y. Yu, H. He, *Chem. Eng. J.* **163**, 62 (2010).
- [20] L. Kong, D. J. Gregg, I. Karatchevtseva, Z. Zhang, M. G. Blackford, S. C. Middleburgh, G. R. Lumpkin, G. Triani, *Cheminform* **53**, 6761 (2014).
- [21] A. Verma, A. G. Joshi, A. K. Bakhshi, S. M. Shivaprasad, S. A. Agnihotry, *Appl. Surf. Sci.* **252**, 5131 (2006).
- [22] N. Răduțoiu, C. M. Teodorescu, *Dig. J. Nanomater. Biostr.* **8**, 1535 (2013).
- [23] M. S. P. Francisco, P. A. P. Nascente, V. R. Mastelaro, A. O. Florentino, *J. Vac. Sci. Technol. A* **19**, 1150 (2001).
- [24] J. Pouilleau, D. Devilliers, H. Groult, P. Marcus, *J. Mater. Sci.* **32**, 5645 (1997).
- [25] M. Iliut, C. Leordean, V. Canpean, C. M. Teodorescu, S. Astilean, *J. Mater. Chem. C* **1**, 4094 (2013).

*Corresponding author: wjzhang@aliyun.com